

Design and fabrication of an electrohydrodynamically actuated microlens with areal density modulated electrodes

This content has been downloaded from IOPscience. Please scroll down to see the full text.

2016 J. Micromech. Microeng. 26 015004

(<http://iopscience.iop.org/0960-1317/26/1/015004>)

View [the table of contents for this issue](#), or go to the [journal homepage](#) for more

Download details:

IP Address: 128.104.78.188

This content was downloaded on 02/12/2015 at 16:07

Please note that [terms and conditions apply](#).

Design and fabrication of an electrohydrodynamically actuated microlens with areal density modulated electrodes

Alireza Ousati Ashtiani and Hongrui Jiang

Department of Electrical and Computer Engineering, University of Wisconsin-Madison, Madison, WI 53706, USA

E-mail: hongrui@engr.wisc.edu

Received 9 July 2015, revised 29 September 2015

Accepted for publication 3 November 2015

Published 30 November 2015



Abstract

In this paper, we introduce an electrode design for electrohydrodynamically actuated liquid microlenses. The effective electrode areal density radially increases which results in centering of the liquid tunable microlens with a planar device structure. A model was developed to demonstrate the centering mechanism of the liquid microlens. 3D electrostatic simulation was conducted and validity of the idea was examined. A simple fabrication process was developed that uses a surface modified SU-8 as the insulator. The focal length of the microlens was measured to vary from 10.1 mm to 5.8 mm as the voltage varied from zero to 100 V.

Keywords: microlens, tunable lens, electrowetting, dielectric lens, MEMS actuator, micro optics, focus tunable lens

(Some figures may appear in colour only in the online journal)

1. Introduction

The advancement of miniaturized imaging systems has brought to life numerous applications in consumer, industrial, and medical fields. From a device perspective, these imaging systems have an optical microlens setup and a light sensor to capture images or videos. Modern CMOS sensors now provide high sensitivity, low noise, low power consumption, low voltage operation, high speed imaging, and good dynamic range [1]. In the area of microlenses, however, very few fundamental advancements have been demonstrated in the past. Most of the miniaturized imaging systems that are equipped with a focusing mechanism are still based on traditional voice coil actuators which have high power consumption, bulky design, and slow response time due to their inherently large structure. In order to fabricate microlenses with low power consumption and a faster response time, various liquid tunable liquid microlenses are being researched with the potential of finding application in future miniaturized optical imaging systems.

Currently, the state of the art focus tunable liquid microlenses rely on various driving mechanisms, including

piezoelectric [2–5], pneumatic [6, 7], dielectrophoresis [8–11], electrowetting (EW) [12–14], hydrogel [15–17], and thermoelectric actuators [18, 19]. All of these liquid microlenses require a method to center the optical axis in order to realize a practical and usable tunable microlens. As a result, most liquid microlenses are still based on non-planar structures [12, 20], which are very difficult to manufacture in a typical fab, compared to a planar configuration. In addition, in applications that require the use of a flexible substrate [21–23], having a non-planar yet flexible electrode structure further complicates the fabrication process and it remains advantageous to develop simpler, planar electrode structures.

In various electrohydrodynamically-driven liquid microlenses, innovative planar structures have been proposed. For example, dielectric-force (DE) based liquid microlenses such as the one reported in [24] use planar, annular ring electrodes that provide droplet centering. This type of design provides digitized tunability since the droplet is pinned at predefined electrode rings. In order to deliver continuous focal length control and to simultaneously implement an intrinsic centering

mechanism, we propose a fully planar electrode design that can be harnessed in both DE-based and EW-based liquid microlenses. Recently [25], we reported preliminary results of this design. Here, we aim to further develop the concept and present a comprehensive study about the electrode structure, fabrication steps, electrostatic simulation, and device characterization.

2. Methods

First, the concept behind the areal density modulated electrodes was developed and a simple analytical model was constructed. Based on the simplified analytical model, a MATLAB® code was compiled to confirm the validity of the idea. From there, an electrostatic simulation was conducted to assess the potential of this design in an EW driven microlens. Then, a fabrication process was devised and developed, based on the conceptual design of the actuator. Finally, the device was fabricated and its optical functionality was demonstrated.

3. Results and discussion

3.1. Concept

Generally speaking, in a given electrohydrodynamic system, the most stable energy state of the whole system will be the state that results in the least amount of potential energy. In a given electrostatically actuated microlens, the well-known Young–Laplace equation dictates a spherical cap shape for the liquid droplet on top of a given surface with a known surface energy [14], which in turn, is controlled by an electrical field. In this regard, for a particular amount of charge applied to the electrodes of an electrohydrodynamically actuated liquid microlens, a favorable droplet position will be defined by droplet placement that causes maximum electrical capacitance since the stored electrical energy would be:

$$U = \frac{1}{2} \frac{q^2}{C}, \quad (1)$$

where U is potential energy, q is stored charge, and C is the capacitance. In the case of the aforementioned EW microlenses [12], maximizing the capacitance on a non-planar device results in centering the microlens. In the proposed design, we aim to find a planar electrode layout that maximizes the capacitance only when the droplet is situated at the center. Such an architecture would have the inherent tendency to force the droplet to be positioned at the center of the microlens structure.

The recommended structure relies on changing the profile of the electrodes. Electrodes are shaped with a radially increasing surface area. Each electrode is placed in a sector, which we call a unit cell, that covers a very small portion of the active device area. (i.e. the central angle of the circular sector that includes each electrode will be a fraction of a radian.) For example, in various designs, we opted for 156, 78, and 48 unit cell structures. The entire device then consists of a number of such electrodes that are arranged in a circular pattern next to

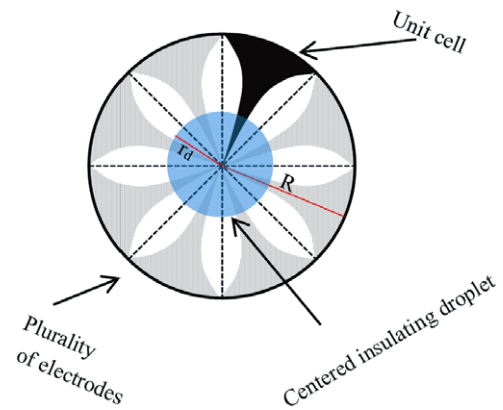


Figure 1. Top view of the electrode design. A plurality of radially extending electrodes is laid next to each other in a circular pattern. A unit cell is highlighted with radially increasing areal density. Black and dotted areas highlight the electrodes, and the white space represents the lateral electrode gap. In the embodiment discussed here, an insulating droplet is placed at the center of the structure which is surrounded by a conductive liquid. In this figure, a design with eight unit cells is shown. In a real device however, a much higher number of electrodes is used.

each other. A top view of a conceptual electrode structure with eight electrodes and a unit cell is shown in figure 1.

As can be seen in figure 1, in a unit cell of the proposed design, the effective electrode areal density that is covered by an electrode increases radially. In other words, in a polar coordinate, a higher radius value corresponds to a higher surface percentage coverage by the electrodes.

In this paper, we examine such an arrangement in an EW microlens. Almost all EW liquid microlenses contain two immiscible liquids where one is an electrical insulator and the other is a conductor. In the proposed arrangement, the liquid at the center is an insulator and the surrounding liquid is a conductive liquid. All electrodes are covered by a thin layer of solid insulating film. Such an arrangement works on the principle of electrowetting on dielectric (EWOD), where one electrode would be the conductive liquid and the counter electrode would consist of the remaining electrodes that are shown. By applying a voltage between the electrodes and the conductive liquid, the contact angle of the conductive-liquid/solid-insulator will change. Furthermore, the resulting capacitor will maximize itself by squeezing the insulating liquid inward. In an EW microlens with a continuous bottom electrode, the insulating droplet might be positioned anywhere because there is no specific favorable droplet position that results in a maximum capacitance. In the proposed design however, since the area is not homogenous, one can anticipate a favorable droplet position that results in the maximum capacitance. Therefore we need to examine the effect of the droplet center position on the capacitance of the device.

3.2. Microlens structure

The cross section of a microlens based on the proposed electrode layout is shown in figure 2. A silicone oil droplet with a refractive index of 1.49 is placed on top of a prefabricated SU-8 micro-stage and is surrounded by an aqueous-based,

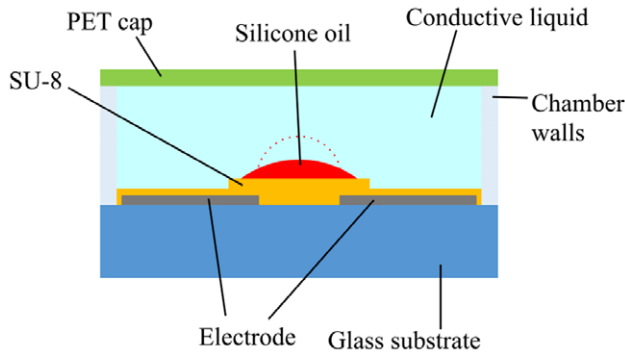


Figure 2. Cross section of the liquid microlens. The insulating liquid, which is silicone oil, is placed on a predefined SU-8 micro-stage. The rest of the chamber is filled with a water-based conductive liquid. By applying a voltage to the electrodes, the silicone oil droplet is radially pushed inward (shown by the dotted red line), and its curvature changes, resulting in a change of the focal length of the microlens. A variable capacitance is seen from the electrodes. It consists of a water-based conductive liquid as a floating electrode that moves on top of insulated electrodes.

floating conductive electrode with a refractive index of 1.35. It is worth noting that contrary to most of the EW designs, we opted to use the conductive liquid as a floating electrode. In this way, the conductive liquid and the circuit are galvanically isolated thereby preventing all associated problems of having a direct electrical contact with the conductive aqueous liquid, for example, microbubbles [26, 27].

Electrodes of the microlens are shown in figure 3. Similar to other reports [28, 29] in this design, an interdigitated electrode structure is used. In our design, we further the benefit of having lateral gaps by intentionally adjusting the gap to create a centering mechanism as stated before. When a voltage is applied to a number of interdigitated electrodes, the curvature of the boundary between these two immiscible liquids is altered. Considering that the droplet volume will not change, the curvature of the centered liquid will be altered. Then, since the refractive indices of the aforementioned liquids are different, the resulting spherical cap will become a microlens. Because the refractive index of the oil droplet is higher, a microlens with a tunable and positive focal length will be the result.

3.3. Capacitance modeling

In order to analyze the device capacitance, we assume that the total capacitance is a linear function of the area that is covered by the conductive-liquid/electrode interface. In a practical device, this would be a sound assumption since the length and width of the electrodes are much larger ($\gg 10$ times greater) than the solid insulator thickness. We can confidently correlate the capacitance between the conductive liquid and each electrode to the common electrode area between them, similar to a parallel plate capacitor. Consequently, we omit fringing electrostatic fields at the edges of the electrodes since the energy stored there will be infinitesimal and will not affect the total electrostatic energy of the device by a measurable margin. As a result, we can say that the total capacitance is a

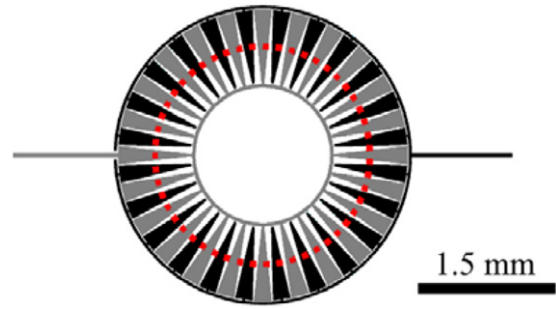


Figure 3. Top view of the electrode design. A number of interdigitated electrodes (shown with black and grey) are connected to a voltage source. The lateral gap between electrodes decreases as a function of radius. The dashed red circle at the center shows the circumference of the oil droplet at the center. For a given droplet diameter, any lateral movement of the droplet will result in a change of the capacitance seen from the electrical circuit due to a radially varying gap between electrodes.

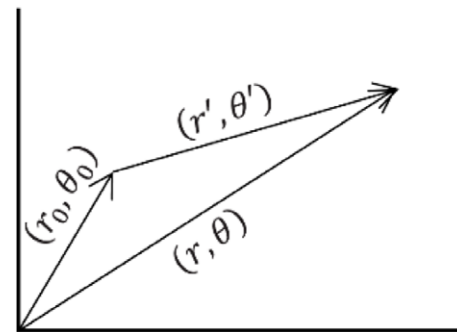


Figure 4. Graphical representation of polar coordinate variable transformation used in deriving the transformed areal density function.

linear function of the total surface area that is covered by the conductive-liquid/electrode interface:

$$C_{\text{total}} = \sum_{i=1}^n \frac{\epsilon A_i^{\text{Cap}}}{d} = \frac{\epsilon A_{\text{Total}}^{\text{Cap}}}{d}, \quad (2)$$

where C_{total} is the total capacitance seen from the circuit, i represents the index for each electrode, A_i^{Cap} is the area between the conductive liquid and electrode i , $A_{\text{Total}}^{\text{Cap}}$ is the total area between the electrodes and the conductive liquid, n is the number of electrodes, ϵ is the permittivity of the solid insulator, and d is the thickness of the solid insulator. In order to calculate the total area that is covered between all the electrodes and the conductive liquid, we calculate the area that is covered by the insulating-liquid/electrodes interface at the middle and subtract its value from the total area of all electrodes. Hence, the total area of conductive-liquid/electrodes interface can be calculated and thus the total capacitance can be deduced.

In a proposed electrode design based on an architecture similar to figure 1, there will be a large number of electrodes. In the unit cell (or circular sector) corresponding to each electrode, a higher fraction of the area is covered by the electrode as we proceed radially outward. In order to better represent the structure, first we define areal density function. This function shows the fraction of the area that is covered by an electrode as a function

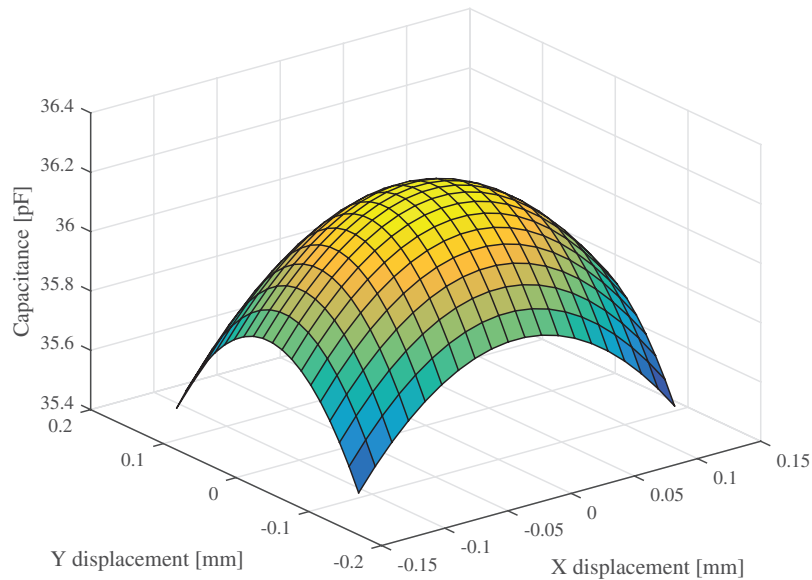


Figure 5. Calculated capacitance as a function of droplet center displacement relative to the center of the device. As displayed here, maximum capacitance occurs when the center of the droplet and device coincide.

of its position. We will limit it to be a function of radius only, and we assume the origin to be at the center of the device. As an example, we define a simple areal density function as follows:

$$F(r) = \begin{cases} \frac{r}{R} & r \leq R \\ 0 & r > R \end{cases}, \quad (3)$$

where r is the radius, R is the outermost radius of electrodes, and $F(r)$ is the areal density function. If the droplet with a radius of r_d remains at the center, total electrode area covered by the insulating droplet will be as follows:

$$A_{\text{total}}^d(0, 0) = \int_{\theta=0}^{2\pi} \int_{r=0}^{r_d} F(r) r dr d\theta, \quad (4)$$

and the whole area of the electrode (which is covered by either the insulating liquid or the conductive liquid) would be A_{total} that can be calculated similar to equation (4). Now if we displace the droplet by (r_0, θ_0) , in order to calculate $A_{\text{total}}^d(r_0, \theta_0)$, we need to determine a new, transformed areal density function. We first define a new coordinate system with the origin shifted to (r_0, θ_0) , and in this new coordinate system with (r', θ') as variables, we can write equation (4) with new variables (r', θ') . With reference to figure 4, the transformed areal density function will become:

$$F^d(r', r_0, \theta_0) = \begin{cases} \frac{\sqrt{r_0^2 + r'^2 + 2r_0r' \cos(\theta_0 - \theta')}}{R} & r' \leq R \\ 0 & r' > r \end{cases} \quad (5)$$

Thereafter, the total effective electrode/insulating-droplet $A_{\text{total}}^d(r_0, \theta_0)$ in a polar coordinate system can be computed. By subtracting $A_{\text{total}}^d(r_0, \theta_0)$ from A_{total} , the value of $A_{\text{Total}}^{\text{Cap}}$ can be calculated as a function of (r_0, θ_0) . Finally, based on equation (2), the capacitance of the circuit can be derived. Since one can define the areal density function in various ways, it

would be very constructive to have a computer code to easily test different areal density functions and the effect they will have on the device capacitance for electrodes with different radii and shapes. Consequently, we developed a MATLAB® code to calculate C_{total} . As an example, an insulating droplet with a radius of 2.5 mm was placed at a center of a number of electrodes with a radius of 3 mm. An areal density function of equation (3) was used in this example. The thickness of the solid insulating layer was assumed to be 2 μm and a relative permittivity of 4.1 (for SU-8 at low frequencies) was used. The results shown in figure 5 indicate, a maximum for $A_{\text{Total}}^{\text{Cap}}$ and as a result, a maximum value for C_{total} occurs when the insulating droplet resides at the center. Furthermore, the rate of capacitance change is higher as the droplet displaces further from the center. This is instructive since it means the restoring force to re-center the droplet will be higher for a larger displacement. To summarize, this model shows that the proposed design has the capability to center the droplet.

3.4. Electrostatic simulation

In the aforementioned capacitance model, some simplifications were made. For example, fringing fields at the edges of electrodes were omitted. In addition, in the case of an interdigitated electrode design, the energy stored in the oil droplet was not considered in the calculation. Although these simplifications are justified, it is instructive to further examine the proposed device structure by conducting a full 3D electrostatic simulation. Coventorware® was used to develop the 3D model of the microlens and geometry was exported to Ansys® Maxwell 3D, which was chosen to further develop 3D electrostatic simulation. Figures 6(a) and (b) show the device geometry used in these simulations. In the model, a droplet was initially placed at the center and then by varying the placement of the center of the droplet, the capacitance was calculated for each instance. In all simulations, the outermost

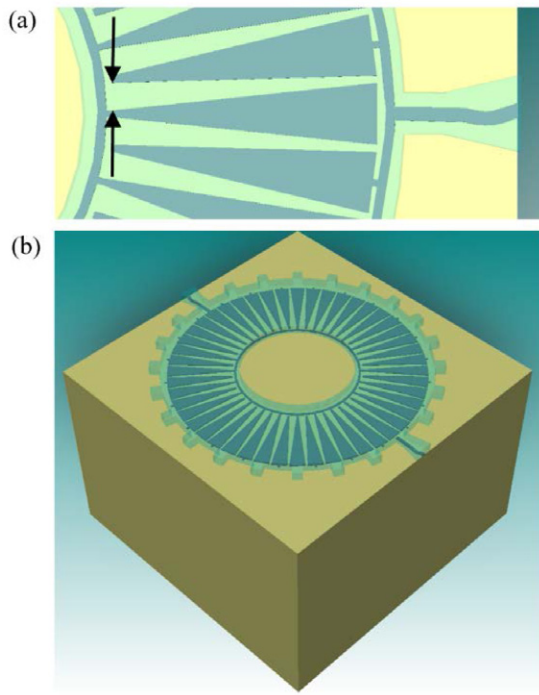


Figure 6. (a) A top view of a section of the microlens showing interdigitated electrodes. The distance between two arrows represents the innermost lateral gap between electrodes. In this case, it is 80 μm . The outermost lateral gap is constant at 20 μm . (b) 3D geometry of the microlens shown in Coventorware[®]. The device thickness is exaggerated by 50 times for better clarity. The shaded green area that has gear shaped bumps is the SU-8 layer. (Oil droplet and the conductive liquid are not shown for better clarity.)

lateral gap, i.e. the gap between interdigitated electrodes at the largest radius of the device, was kept constant at 20 μm . Furthermore, the effect of varying the innermost lateral gap between electrodes was evaluated. From this 3D electrostatic simulation, the capacitance was derived which showed it to be a function of both the innermost lateral gap and the droplet displacement.

The results of the electrostatic simulation are shown in figure 7(a), which displays the voltage distribution in the mid slice of the insulator (SU-8) that sits on top of the electrodes. As can be seen, the voltage is very uniform across areas on top of each electrode and counter electrode, which shows that the assumption of approximating the device with a number of parallel plate capacitors is valid. Furthermore, the average calculated capacitance for both models (simplified parallel plate capacitor model and a full 3D simulation) is in the same range of 35 pF which further confirms the accuracy of the simplified model. Figure 7(b) shows the results of a parametric study in which the innermost lateral gap between the electrodes was varied from 10 μm to 80 μm . In this study, the capacitance was calculated as a function of both the innermost lateral gap between the electrodes and the droplet displacement. As is seen, a wider innermost lateral gap results in a higher capacitance change rate (i.e. the slope of the capacitance function becomes larger). If we consider an analogy to an elastic body, we can define stiffness as:

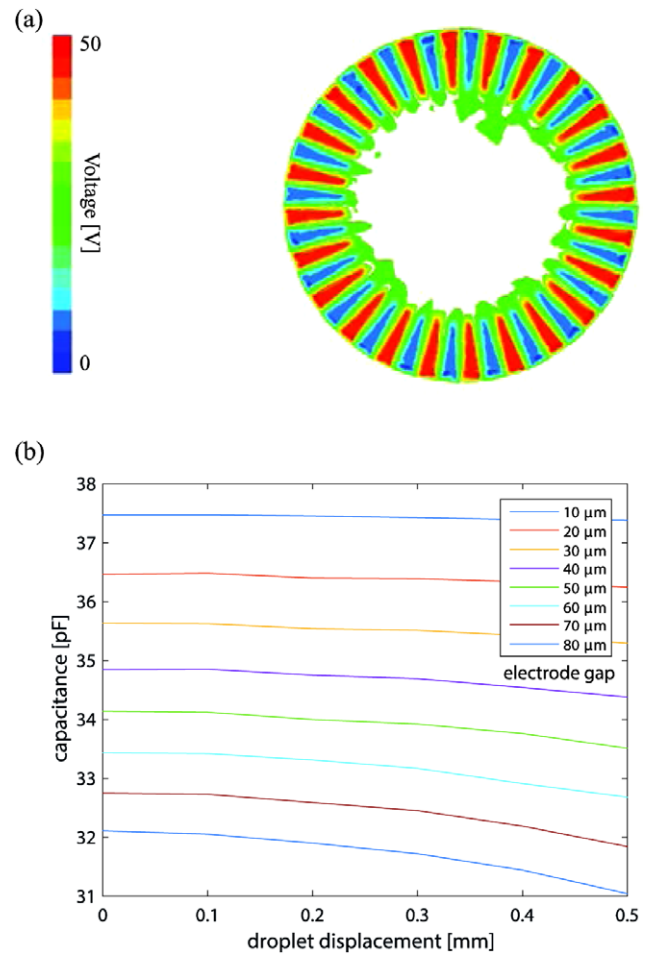


Figure 7. (a) Electrostatic simulation, showing voltage distribution at mid slice through the insulator and on top of the electrodes. (b) Calculated capacitance as a function of droplet displacement for various innermost lateral gaps. For a larger gap variation, the rate of capacitance change becomes higher.

$$K(r) = \frac{F}{r} = \left(\frac{dU(r)}{dr} \right) \frac{1}{r} = \frac{q^2}{2C^2(r)} \frac{dC(r)}{dr} \frac{1}{r}. \quad (6)$$

Hence for a given droplet displacement of r , a higher $\frac{dC(r)}{dr}$ equals a stiffer, stronger droplet centering mechanism. This result shows that a larger innermost lateral gap is preferred and will provide a more robust design.

3.5. Device fabrication

Device fabrication was conducted mostly at the Wisconsin Center of Applied Microelectronics (WCAM) cleanroom of the University of Wisconsin-Madison. Due to the planar nature of the electrodes and substrate, a moderately equipped surface micromachining facility has enough capability to fabricate the proposed microlens. The manufacturing process is shown in figures 8(a)–(e). After cleaning a 100mm fused silica glass, 200nm of aluminum–chromium (Al/Cr) alloy was sputtered onto it. Chromium was added to aluminum to decrease surface roughness, as is indicated in figures 9(a) and (b). As a result, the Al/Cr layer was not impaired by a cloudy surface and did not diffuse the reflection that

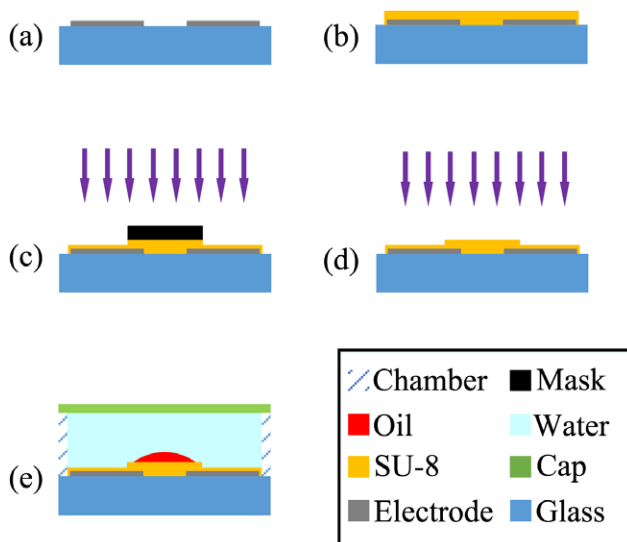


Figure 8. (a) A 200 nm Al/Cr layer was laid onto the glass substrate and patterned. (b) A 2 μm SU-8 layer was spun coated and subsequently patterned. (c) A selective oxygen plasma etching was performed to partially remove SU-8 and create a micro-stage for initial oil droplet placement. (d) An oxygen plasma treatment was conducted to increase the surface roughness of SU-8, followed by SF₆ plasma treatment to create a hydrophobic surface. (e) The device was packaged, filled with a silicone oil droplet at the center and then an aqueous water solution filled the chamber. Finally, a polyethylene terephthalate (PET) cap was placed on top of the chamber to seal the microlens.

would result from a thick aluminum layer. After photoresist (PR) deposition and patterning via contact lithography, the Al/Cr layer was etched in a conventional aluminum wet bench. Residuals of PR were removed by plasma ashing.

One of the main challenges that was solved during the fabrication process engineering was finding a proper SU-8 process flow. In the first step, an adhesion promotion layer was added since SU-8 does not have enough adhesion to either glass or Al/Cr. A diluted SU-8 2000.1 was first spun-coated onto the substrate, and without pre-exposure baking, it was activated via flood exposure (600 mJ cm^{-2}), then was baked at 75°C for 3 min which was followed by hard baking at 150°C for 15 min. This 100 nm, fully cross linked SU-8 layer substantially increased adhesion between subsequent SU-8 and the substrate. In the next step, a $2.5 \mu\text{m}$ SU-8 2002 (MicroChem Corp., 200 Flanders Road Westborough, MA 01581, USA) was deposited and patterned. This SU-8 layer acted as an insulator covering all conductive areas and preventing the aqueous solution from shorting the circuit. Additionally, to fabricate a micro-stage for the oil droplet and prevent oil from creeping onto the glass substrate, the SU-8 layer at the middle was covered by PR and the uncovered areas of SU-8 were partially etched with oxygen plasma. After PR removal, in the subsequent step the wafer was diced and each die was thoroughly washed. (Wafer dicing was intentionally performed in the middle of the fabrication process since it was found that dicing at the final step would alter the surface properties of the SU-8. We attribute this to particle contamination that occurs during dicing.)

Since the SU-8 was initially very smooth and slightly hydrophilic after post exposure baking and had a contact angle of 81° [30], we opted for a fluorine-based surface treatment to make it hydrophobic. However, during our experiments, it became clear that a purely fluorine rich plasma treatment was not enough to fabricate a high quality hydrophobic surface. Thus a two-step surface treatment to fabricate a hydrophobic SU-8 surface was devised. In the first surface treatment step, naked dies were exposed to 5 min of oxygen/argon plasma. As stated elsewhere [31], oxygen plasma treatment increases the surface roughness of SU-8, but renders it hydrophilic. In the next step, a fluorine-rich plasma treatment with sulfur hexafluoride (SF₆) was conducted for 5 min which converted the SU-8 surface to a hydrophobic surface with a contact angle of more than 120° . As can be seen in figure 9(c), the resulting surface showed a nano-mountain shaped structure with a height of around 200 nm. (We attribute increased hydrophobicity of the SU-8 to the increased surface roughness as a result of oxygen treatment and subsequent fluorination of its surface with SF₆ plasma.) SU-8 thickness in the active areas was reduced to around 2 μm after this step. A finalized die is shown in figure 10(a).

After die fabrication, a chamber made from copper washers with an inner diameter of 6 mm and thickness of 2 mm were glued to the die, as shown in figure 10(b). Then 1 μl of silicone oil (DOW CORNING® 550 FLUID, Dow Corning Corporation, Corporate Center, PO Box 994, MIDLAND, MI, 48686-0994, United States) was dispensed at the center and the remainder of the package was filled with a density-matched aqueous solution to prevent buoyancy forces. Then, electrical wires were attached to the device using silver epoxy. Finally, the packaging was completed and the chamber was sealed with a PET cap that was placed on top of the chamber.

3.6. Experiments

After the device fabrication, an optical setup [18] was assembled to measure the focal length. A 10 kHz square wave power supply was connected to the microlens and peak voltage was varied from 0 to 100 volts. As illustrated in figure 11, back focal length (BFL) of the microlens varied from 10.1 mm to 5.8 mm as the voltage sweep ranged from zero to 100 V. Both increasing and decreasing input voltages were applied to observe the effect of hysteresis on the BFL of the microlens. A lagging BFL was observed for a decreasing voltage curve, pointing to a possible contact angle hysteresis which is similar to various EW based devices. Furthermore, in order to see the centering mechanism in action, a top view shape of the droplet was captured using a microscope for an actuation voltage range of 0 to 100 V. As can be seen in figure 12(a), initially with no applied voltage, the droplet was pinned at the edge of the SU-8 micro-stage. When the voltage was applied, the conductive aqueous solution progressed towards the center which squeezed the oil droplet. As a result, the curvature of the oil droplet was changed and the oil droplet edge was axisymmetrically moved towards the center, as evidenced in figures 12(b)–(d). These experiments confirmed that the microlens had a tunable curvature and thus a tunable

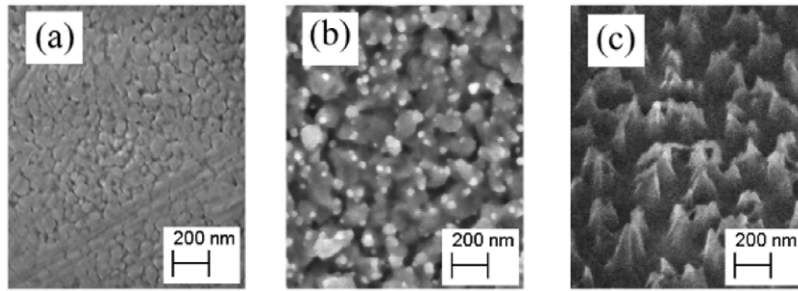


Figure 9. SEM images taken from the surface of the fabricated device. (a) Al/Cr deposited film exhibited a smooth surface and specular light reflection. (b) Pure Al deposited film showed a rough surface and diffuse light reflection which reduced the image contrast in the photolithography process. Thus it was discarded in favor of Al/Cr for device fabrication. (c) SU-8 surface after oxygen/SF6 plasma treatment. Nano mountain-shaped structures with a height of around 200 nm were visible.

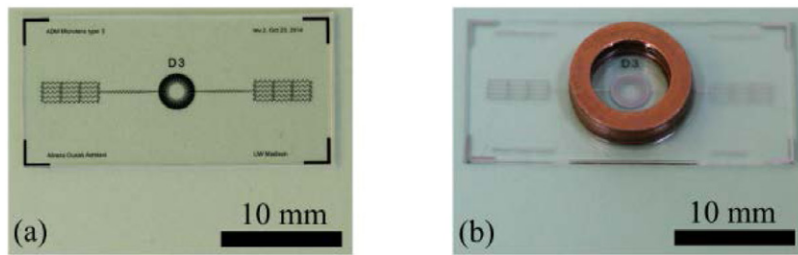


Figure 10. (a) A naked device die. Wavy patterns on electrodes are implemented to make them more compliant on flexible substrates. (b) A fabricated device before adding liquids and sealing, with copper chamber shown. The height of the chamber is 2 mm.

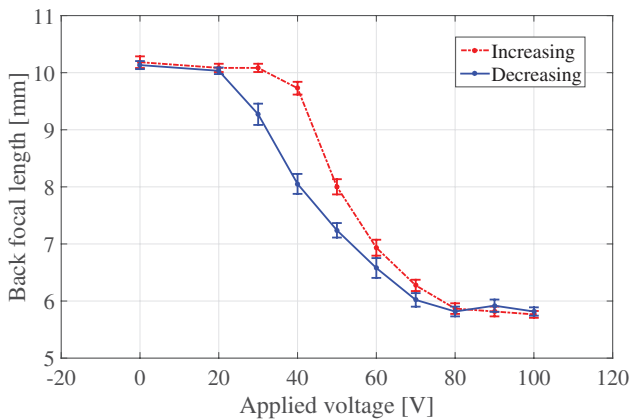


Figure 11. Measured BFL as a function of voltage. Both increasing and decreasing input voltages were applied and hysteresis was observed. Additionally, error bars are shown at various applied voltages.

focal length, while retaining its optical axis and remaining axisymmetric.

In another arrangement, an object was placed under the microlens and the projected image was captured using a microscope. As shown in figures 13(a)–(d), image defocusing occurred when the voltage changed from zero to 80V. In figure 13(e), the resulting image was refocused with the microscope. This focused image clearly demonstrates a change in the image size compared to figure 13(a), confirming the fact that the curvature and thus the focal length of the microlens was changed during actuation. Therefore, a tunable liquid microlens was achieved.

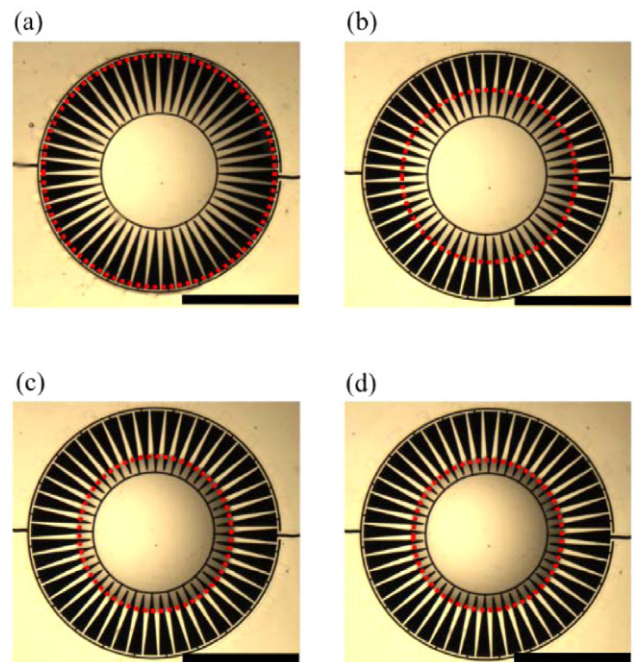


Figure 12. Top view of the microlens at different actuation voltages. All scale bars are 1.5 mm. Dashed circles are added to highlight the edge of the droplet. (a) Initially, the droplet was pinned at the edge of the micro-stage. (b) At 30V, the droplet is centered and the curvature of the droplet is altered. (c) The centered droplet at 60V. (d) The centered droplet at 100V.

In order to characterize microlens resolution, a 1951-USAF target was placed at 48 mm distance from the microlens with an aperture diameter of 1.5 mm. A diffraction-limited

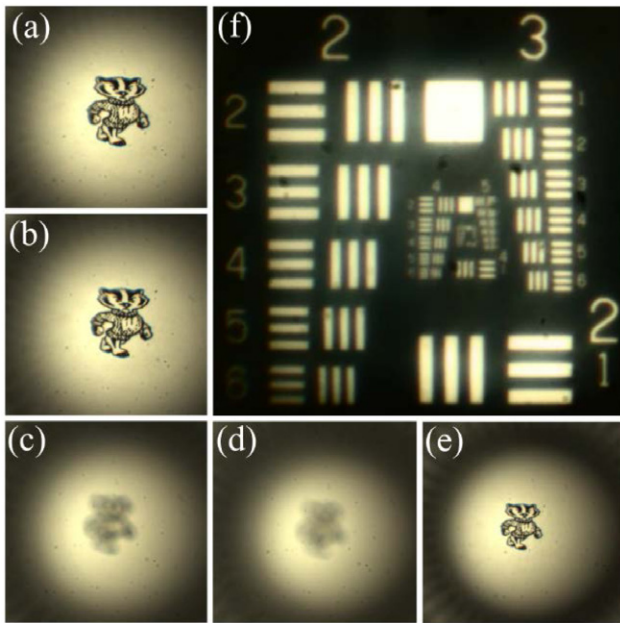


Figure 13. Captured images through a microscope and the microlens at various voltages. (a) 0V. (b) 40V. (c) 60V. (d) 80V. (e) Refocused image via microscope, at 80V. (f) Image of the 1951-USAF resolution chart, captured at 0V. The microlens is capable of resolving group 4, element 4, which corresponds to a resolution of 22.63 lp mm^{-1} .

microlens has an angular resolution, θ , according to the following formula:

$$\theta = 1.22 \frac{\lambda}{D}, \quad (7)$$

where λ is the wavelength and D is the microlens aperture diameter. Assuming $\lambda = 500 \text{ nm}$, the microlens would show a diffraction limited resolution of 0.407 mrad , or 25.61 lp mm^{-1} . As seen in figure 13(f), the microlens is capable of resolving group 4, element 4, which corresponds to a resolution of 22.63 lp mm^{-1} . This shows that the microlens has a small amount of aberration and operates acceptably close to a diffraction limited regime. Considering the very small aperture size of the microlens, this result is anticipated and the loss of resolution is mostly due to diffraction from the aperture.

4. Conclusion

A tunable liquid microlens with a planar electrode structure is highly desired since it is easy to fabricate in readily available clean room facilities around the world. In order to realize such a tunable microlens, we developed the concept of areal density modulated electrodes for microlens. Both simplified and 3D electrostatic simulations were conducted and a favorable centered position for the droplet was displayed. A fabrication method that harnesses readily available SU-8 epoxy as an insulator was developed and the assembled microlens showed both tunable focal length and centering of the liquid microlens. This simplified, planar structure enabled us to fabricate tunable microlenses that can be used in both EW and dielectrophoretic designs. In future efforts, we aim to further

analyze the optical characteristics of the proposed microlens, including measurement of various aberrations. In addition, we plan to conduct a sensitivity analysis of various electrode parameters, to find an optimal electrode shape which gives the maximum centering force and at the same time can be actuated with minimum voltage. We are also planning to extend the same fabrication process to a flexible substrate since the proposed fabrication method can be readily implemented onto flexible structures. Finally, we plan to use a multi-electrode actuation mechanism that can be used to control and compensate for optical aberrations which will have applications in vision correction and future generation contact lenses.

Acknowledgments

This work was supported by the U.S. National Institute of Health (Grant No. 1DP2OD008678-01). This research utilized the US National Science Foundation supported shared facilities at the University of Wisconsin. The authors would like to thank Dr M Moghimi, Dr A Kanhere and Dr C Li for technical discussions and help. The authors are grateful to Mr R Noll at the Materials Science Center at the University of Wisconsin-Madison for help and support in acquiring SEM images. We would like to further thank Professor Behdad's group of the University of Wisconsin-Madison for access and help with using electromagnetic simulation software.

References

- [1] Bigas M, Cabruja E, Forest J and Salvi J 2006 Review of CMOS image sensors *Microelectron. J.* **37** 433–51
- [2] Oku H, Hashimoto K and Ishikawa M 2004 Variable-focus lens with 1 kHz bandwidth *Opt. Express* **12** 2138
- [3] Draheim J, Burger T, Korvink J G and Wallrabe U 2011 Variable aperture stop based on the design of a single chamber silicone membrane lens with integrated actuation *Opt. Lett.* **36** 2032
- [4] Wapler M C, Sturmer M and Wallrabe U 2014 A compact, large-aperture tunable lens with adaptive spherical correction *2014 Int. Symp. on Optomechatronic Technologies* pp 130–3
- [5] Zuerbig V *et al* 2013 Piezo-actuated tunable diamond/AlN micro lenses *2013 Transducers & Eurosensors XXVII: The 17th Int. Conf. on Solid-State Sensors, Actuators and Microsystems (TRANSDUCERS & EUROSENSORS XXVII)* pp 2317–20
- [6] Werber A and Zappe H 2008 Tunable pneumatic microoptics *J. Microelectromech. Syst.* **17** 1218–27
- [7] Werber A and Zappe H 2005 Tunable microfluidic microlenses *Appl. Opt.* **44** 3238–45
- [8] Ren H and Wu S-T 2008 Tunable-focus liquid microlens array using dielectrophoretic effect *Opt. Express* **16** 2646–52
- [9] Ren H, Xianyu H, Xu S and Wu S-T 2008 Adaptive dielectric liquid lens *Opt. Express* **16** 14954–60
- [10] Cheng C-C, Chang C A and Yeh J A 2006 Variable focus dielectric liquid droplet lens *Opt. Express* **14** 4101–6
- [11] Cheng C-C and Yeh J A 2007 Dielectrically actuated liquid lens *Opt. Express* **15** 7140–5
- [12] Berge B, Normale E, De Lyon S and France L 2005 Liquid lens technology: principle of electrowetting based lenses and applications to imaging *18th IEEE Int. Conf. on Micro Electro Mechanical Systems, 2005. MEMS 2005* pp 227–30

- [13] Berge B and Peseux J 2000 Variable focal lens controlled by an external voltage: an application of electrowetting *Eur. Phys. J. E* **3** 159–63
- [14] Mugele F and Baret J 2005 Electrowetting: from basics to applications *J. Phys. Condens. Matter* **17** R705–74
- [15] Dong L, Agarwal A K, Beebe D J and Jiang H 2006 Adaptive liquid microlenses activated by stimuli-responsive hydrogels *Nature* **442** 551–4
- [16] Dong B L, Agarwal A K, Beebe D J and Jiang H 2007 Variable-focus liquid microlenses and microlens arrays actuated by thermoresponsive hydrogels *Adv. Mater.* **19** 401–5
- [17] Zhu D, Lo C, Li C and Jiang H 2012 Hydrogel-based tunable-focus liquid microlens array with fast response time *J. Microelectromech. Syst.* **21** 1146–55
- [18] Ashtiani A O and Jiang H 2014 Tunable microlens actuated via a thermoelectrically driven liquid heat engine *J. Appl. Phys.* **115** 243103
- [19] Ashtiani A O and Jiang H 2013 Thermally actuated tunable liquid microlens with sub-second response time *Appl. Phys. Lett.* **103** 111101
- [20] Kuiper S and Hendriks B H W 2004 Variable-focus liquid lens for miniature cameras *Appl. Phys. Lett.* **85** 1128–30
- [21] Li C and Jiang H 2014 Fabrication and characterization of flexible electrowetting on dielectrics (EWOD) microlens *Micromachines* **5** 432–41
- [22] Lu Y-S, Tu H, Xu Y and Jiang H 2013 Tunable dielectric liquid lens on flexible substrate *Appl. Phys. Lett.* **103** 261113
- [23] Li C and Jiang H 2012 Electrowetting-driven variable-focus microlens on flexible surfaces *Appl. Phys. Lett.* **100** 231105
- [24] Tsai C G, Chen C-N, Cheng L-S, Cheng C-C, Yang J-T and Yeh J A 2009 Planar liquid confinement for optical centering of dielectric liquid lenses *IEEE Photonics Technol. Lett.* **21** 1396–8
- [25] Ashtiani A O and Jiang H 2015 An electrohydrodynamically actuated liquid microlens with areal density modulated electrodes *18th Int. Conf. on Solid-State Sensors, Actuators and Microsystems* pp 2089–92
- [26] Chung S K, Zhao Y and Cho S K 2008 On-chip creation and elimination of microbubbles for a micro-object manipulator *J. Micromech. Microeng.* **18** 095009
- [27] Cooney C G, Chen C-Y, Emerling M R, Nadim A and Sterling J D 2006 Electrowetting droplet microfluidics on a single planar surface *Microfluid. Nanofluidics* **2** 435–46
- [28] Xu M, Xu D, Ren H, Yoo I-S and Wang Q-H 2014 An adaptive liquid lens with radial interdigitated electrode *J. Opt.* **16** 105601
- [29] Yang S, Krupenkin T N, Mach P and Chandross E A 2003 Tunable and latchable liquid microlens with photopolymerizable components *Adv. Mater.* **15** 940–3
- [30] del Campo A and Greiner C 2007 SU-8: a photoresist for high-aspect-ratio and 3D submicron lithography *J. Micromech. Microeng.* **17** R81–95
- [31] Walther F, Davydovskaya P, Zürcher S, Kaiser M, Herberg H, Gigler A M and Stark R W 2007 Stability of the hydrophilic behavior of oxygen plasma activated SU-8 *J. Micromech. Microeng.* **17** 524–31